Nordic Overturning Increases as AMOC Weakens in Response to Global Warming

Sasha Roewer[1,2], Lukas Fiedler[1,2,3], Marius Årthun[4], Willem Huiskamp[1], and Stefan Rahmstorf[1]

[1]RD1- Earth System Analysis, Potsdam-Institute for Climate Impact Research (PIK), Member of the Leibniz Association, Potsdam, Brandenburg, Germany
[2]current affiliation: IMPRS-ESM, Max Planck Institute for Meteorology, Hamburg, Germany
[3]current affiliation: Institute of Oceanography, Center for Earth System Research and Sustainability, University of Hamburg, Hamburg, Germany
[4]Geophysical Institute, University of Bergen, and Bjerknes Centre for Climate Research, Bergen, Norway

Correspondence: Sasha Roewer (sasha.roewer@mpimet.mpg.de)

Abstract. The Atlantic Meridional Overturning Circulation (AMOC) is weakening in response to global warming, while Nordic Seas Overturning Circulation (NOC) is projected to increase. So far, no causal link has been proposed between these two opposing trends. Here we propose that a density reduction in the subpolar North Atlantic will weaken the AMOC by reducing the density difference with lighter waters further south, while at the same time strengthening the NOC by increasing the density difference with the heavier waters further north. Using high resolution climate model data and a box model, we
5   find that in response to combined global warming and freshwater input the NOC initially increases moderately as the AMOC weakens, while a tipping point may be reached later if deep convection in the Nordic Seas shuts down and the NOC collapses together with the AMOC.

1 Introduction

10   The Atlantic Meridional Overturning Circulation (AMOC) is an important feature of the Earth's climate system. The one petawatt of energy it transports northward (Trenberth and Fasullo, 2017) warms the entire Northern Hemisphere, in particular around the northern Atlantic mid to high latitudes. The northward branch of the current system extends across the Greenland-Scotland Ridge (GSR), which separates the North Atlantic Ocean from the Nordic Seas and the Arctic Ocean. Warm, saline water is transported into the Nordic Seas, where it loses heat to the atmosphere (Bosse et al., 2018; Mauritzen, 1996), leading

15   to the formation of dense overflow waters that return to the North Atlantic across the GSR, contributing significantly to the deep limb of the AMOC (Dickson and Brown, 1994; Hansen and Østerhus, 2000). In the following, we will call the branch of the circulation north of and flowing across the GSR the Nordic Overturning Circulation (NOC) and the part south of the GSR the AMOC for clarity.

20   A primary source of North Atlantic Deep Water (NADW) and key driver of the AMOC is convection in the subpolar North Atlantic and Nordic Seas (Kuhlbrodt et al., 2007; Dickson and Brown, 1994). The main convection sites are located in the

Irminger Sea, Labrador Sea and Nordic Seas. In the subpolar North Atlantic, heat loss to the atmosphere due to strong winds and low winter temperatures increases the density of surface waters (Marshall and Schott, 1999; Pickart et al., 2003), while in the Nordic Seas, specifically the Greenland Sea, brine rejection during sea ice formation plays an additional role in the triggering of deep convection (Roach et al., 1993; Rudels, 1990). It has been argued that in response to buoyancy changes in the subpolar North Atlantic (e.g. because of surface warming in combination with reduced northward salt advection under a weakened AMOC (Drijfhout et al., 2025)), convection in the northern Atlantic might weaken or shut down, reducing the volume transport of the AMOC.

There is evidence that the AMOC has weakened since the mid-twentieth century (Dima and Lohmann, 2010; Drijfhout et al., 2012; Zhu and Liu, 2020; Caesar et al., 2021; Zhu et al., 2023; Ren et al., 2025; Li and Liu, 2025), due to anthropogenic emissions (Chemke et al., 2020; Dagan et al., 2020; Qasmi, 2023). Observations show a trend of declining density in the Irminger Sea which is well above 90% significant despite large internal variability, though just short of the 95% mark. This corresponds dynamically to a 13% AMOC weakening (Chafik et al., 2022), in line with other estimates, e.g. Caesar et al. (2018). In several hosing (Stouffer et al., 2006; Jackson et al., 2023; van Westen et al., 2025a) or CO_2 (Gregory et al., 2005; Weaver et al., 2007; Weijer et al., 2020; Drijfhout et al., 2025) forcing experiments, the AMOC has demonstrated the capacity to slow or even shut down completely on centennial time scales, with consequences for both regional and global climate. If the AMOC were to shut down, the temperature in Europe could cool by several degrees, with more extreme cold events in winter (van Westen et al., 2024), particularly in northern Europe and Scandinavia. In contrast, the Southern Hemisphere would warm over multi-decadal timescales due to reduced northward heat transport (Vellinga and Wood, 2002; Diamond et al., 2025; van Westen et al., 2025a). Additional impacts include a southern shift of the Intertropical Convergence Zone (Vellinga and Wood, 2002; van Westen et al., 2024), large-scale sea level rise in the North Atlantic (Levermann et al., 2005), wide-ranging impacts between ocean basins such as a strengthening of the Walker circulation (Orihuela-Pinto et al., 2022), a strengthening of the North Atlantic storm tracks, a decrease in summer precipitation across much of Europe as well as a decrease in vegetation and crop productivity (Jackson et al., 2015; van Westen et al., 2025b), to name a few.

Contrary to the AMOC's response to buoyancy changes forced by surface warming or increased freshwater input, a future strengthening of the NOC is predicted in global climate models (Årthun et al., 2023). This increased overturning takes place as anomalously warm and salty surface waters translate into changes in water mass transformation and horizontal circulation. Surface density changes in the Nordic Seas also affect the NOC by altering the pressure gradient across the GSR, and, hence, the exchanges between subpolar North Atlantic and the Nordic Seas (Olsen et al., 2008; Chafik et al., 2025). Similarly, density changes south of the GSR can also drive changes in the NOC. Specifically, Chafik et al. (2025) demonstrated that on multi-year timescales AMOC-driven temperature anomalies in the subpolar North Atlantic modulate the pressure gradient and overturning across the GSR; a stronger AMOC leading to a stronger NOC. But how then does this coherent connection between large-scale circulation changes (i.e., the AMOC) and Nordic Seas overturning variability, relate to the opposing future trajectories of the AMOC and the NOC?

Here, we investigate the hypothesis that, since the NOC, similarly to the AMOC, is impacted by the density difference across the GSR, increased freshwater forcing in the northern Atlantic could increase the NOC by increasing the density gradient be-
60   tween the northern Atlantic and the Nordic Seas. This would in turn enhance the heat transport into the Nordic Seas and Arctic Ocean, consistent with future projections (Shu et al., 2022; Dörr et al., 2024). This study aims to investigate the increase of heat transport into the Nordic Seas and overturning, and its possible connection to a weakening AMOC under global warming conditions. Using high resolution climate model data and an idealized box model, we isolate the density-driven dynamics and feedbacks connecting the AMOC and NOC.

2   Methods

2.1   Climate Model Simulations With CM2.6

This study employs the GFDL CM2.6 climate model, a high-resolution Coupled General Circulation Model (CGCM) developed by the Geophysical Fluid Dynamics Laboratory (GFDL) (Griffies et al., 2015; Saba et al., 2016). CM2.6 consists of the AM2 atmosphere, LM3 land model, MOM5 ocean model, and SIS sea ice model. The atmosphere and land models have a
70   lateral resolution of nominally 0.5 C$^\circ$ with AMS utilising 32 vertical layers. MOM5, as implemented in CM2.6, features a refined ocean resolution varying from 11 km at the equator to 4 km at high latitudes, allowing for an eddy-permitting representation of ocean dynamics (Delworth et al., 2012). The model includes 50 vertical layers in re-scaled geopotential height (z^*) coordinates, over 5500m.

This model was selected for several reasons. Griffies et al. (2015) demonstrated that CM2.6 realistically captures transient
75   mesoscale eddy heat transport in the northern Atlantic, allowing a clear separation between the contributions of mean advection and eddy processes. This leads to a more accurate representation of how heat converges within the ocean interior and results in smaller temperature drifts and more stable global heat budgets over long integrations. Similarly, Saba et al. (2016) showed that CM2.6 reproduces the pathways and interactions of the Northwest Atlantic circulation with much greater fidelity,
80   yielding more realistic regional climate change projections. In the Arctic context, Decuypère et al. (2022) found that CM2.6 provides the best agreement with observed ocean heat transport and represents inter-basin heat transport more accurately than medium- and low-resolution models from the same model suite. In summary, these findings indicate that CM2.6 offers a robust framework for investigating northern Atlantic ocean heat transport processes and their evolution under elevated CO_2 concentrations.

85

Experimental Design The model is initialized with preindustrial boundary conditions, including atmospheric CO_2 concentration of 280 ppm as well as observed present-day ocean-conditions (Steele et al., 2001). Two experiments are performed subsequently derived from this initial simulation. In the preindustrial control run (PIC), atmospheric CO_2 concentrations are kept constant at 280 ppm for 80 years, maintaining stable preindustrial climate conditions. In the CO_2 doubling experiment

90 (2xCO$_2$), atmospheric CO$_2$ is increased by 1% per year over a period of 70 model years, reaching a final concentration of 560 ppm. The simulation is then extended for an additional 10 years with CO$_2$ levels held constant, allowing the system to adjust under the increased greenhouse gas forcing (Delworth et al., 2012). For this study, output from the last 20 years of each simulation is used.

2.2 Calculating Meridional Heat Transport

95 To calculate the meridional heat transport (MHT) across a desired latitude, a net zero volume transport is required (Bryden and Imawaki, 2001). Hence, the zero-velocity reference is utilised to estimate the geostrophic velocities. The section-averaged velocity is then subtracted from the velocity field. We compute MHT as follows:

$$MHT = \rho_0 C_p \int\limits_x \int\limits_z \Theta(x,z)\big[v(x,z) - \bar{v}\big]dxdz \; , \tag{1}$$

with $\bar{v}$ being the mean velocity over the cross section for the full basin depth. This ensures that MHT is associated with a net 100 zero volume transport and therefore independent of a reference temperature (Bryden and Imawaki, 2001).

2.3 Decomposing Meridional Heat Transport

2.3.1 Dynamic-Thermodynamic Decomposition

To analyse the meridional heat transport (MHT) anomalies, we compute the differences in MHT between the two CM2.6 simulations (MHT'). These anomalies are decomposed following the methodology of Bony et al. (2004), attributing changes to 105 thermodynamic effects (associated with anomalous temperature variations), dynamic effects (related to changes in circulation), and non-linear interactions between the two. In the following, these components are referred to as thermodynamic, dynamic, and non-linear contributions, respectively. We set up the dynamic-thermodynamic decomposition as:

$$MHT' = \rho_0 C_p \Big[\overbrace{\int\limits_x \int\limits_z \bar{v}\Theta' dxdz}^{\text{thermodynamic}} + \overbrace{\int\limits_x \int\limits_z \bar{\Theta}v' dxdz}^{\text{dynamic}} + \overbrace{\int\limits_x \int\limits_z \Theta'v' dxdz}^{\text{non-linear}} \Big] \tag{2}$$

Here, bars denote variables from the PIC simulation, while primes indicate anomalies from the 2xCO$_2$ run relative to the 110 PIC run, such that $\bar{v} = v_{\text{PIC}}$, $\overline{\Theta} = \Theta_{\text{PIC}}$, $v' = v_{2\text{xCO}_2} - v_{\text{PIC}}$ and $\Theta' = \Theta_{2\text{xCO}_2} - \Theta_{\text{PIC}}$. Following the approach of Oldenburg et al. (2018), the thermodynamic component of MHT' represents the advection of anomalous heat by the mean circulation, the dynamic component corresponds to the advection of mean heat by anomalous currents, and the non-linear contribution arises from simultaneous changes in both temperature and circulation.

2.3.2 Overturning-Gyre Decomposition

115 Following Bryan (1982), MHT in the northern Atlantic can be decomposed into contributions from the two dominant gyre systems, the subpolar gyre south of Greenland and the weaker gyre in the Nordic Seas, as well as from the overturning
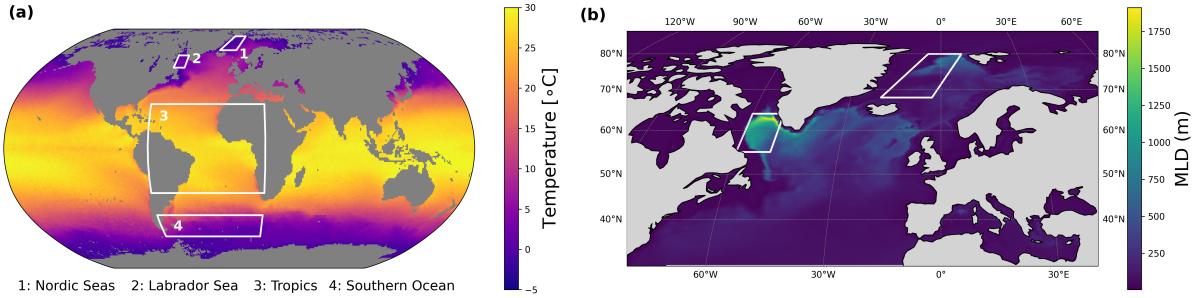
Figure 1. (a) Mean sea surface temperature during winter 1971-2000 from WOA23 (Reagan et al., 2024). The temperatures used for the tuning process were averaged across the outlined regions. (b) ORAS5 mixed layer depth (MLD) data (Copernicus Climate Change Service, 2021) for the subpolar North Atlantic and Nordic Seas. The region used for averaging temperature include the convection sites. The co-ordinates for the areas are: Southern Ocean: 70°S - 45°S, 60°W-20°E; Tropics: 30°S - 30°N, 70°W-20°E; Labrador Sea: 55°N - 64°N, 50°W-60°W; Nordic Seas: (20°W, 68°N), (3°W, 68°N), (8°E, 80°N), (5°W, 80°N)

circulation. We compute the gyre contribution to MHT as:

$$MHT_{\mathrm{gyre}} = \rho_0 C_p \int\limits_x \int\limits_z \langle \Theta^* \rangle \langle v^* \rangle dx dz \; , \tag{3}$$

and the overturning contribution to MHT as:

$$MHT_{\mathrm{overturning}} = \rho_0 C_p \int\limits_x \int\limits_z \langle \Theta \rangle \langle v \rangle dx dz \; . \tag{4}$$

Here, $\langle \cdot \rangle$ denotes zonal average of the variable and $\langle \cdot^* \rangle$ represents the anomaly from that zonal average.

We acknowledge that at high latitudes a substantial fraction of the overturning occurs through horizontal or gyre circulation across sloping isopycnals, rather than purely vertical exchange. Consequently, the physical interpretation of the overturning and gyre terms in these regions differs from that at lower latitudes (Zhang and Thomas, 2021), even though the mathematical decomposition itself remains valid.

2.4 Box Model

The box model used for the following analysis consists of eight boxes. Box 0 represents the Southern Atlantic and the connection to other ocean basins. Boxes 1, 7, and 6 represent the tropical surface waters, intermediate waters, and deep water regions, respectively. Boxes 2 and 5 cover the surface and deep waters of the northern Atlantic while boxes 3 and 4 represent the Nordic Seas. Convection is active between the surface and bottom waters of the Nordic and northern Atlantic boxes as long as the density stratification is unstable, that is if $\rho_2 > \rho_5$ or $\rho_3 > \rho_4$. The overturning rates, m_0 and m_1, are governed by the density gradients between boxes 0 and 2/5, and 2/5 and 3/4, respectively. m_0 represents the AMOC, and m_1 the Nordic Overturning Circulation (NOC). We use a non-linear approximation for the equation of state (EOS) analogous to (Nycander et al., 2015) to account for the non-linear effects of the temperature on the density at temperatures close to or below zero. Furthermore, all

surface boxes lose or gain heat, governed by the temperature difference between the boxes and a respective restoring temperature multiplied by the restoring rates λ_i. This exchange can be interpreted as heat exchange with the atmosphere. The values for the restoring rates are calculated as follows

$$\lambda_i = \frac{\gamma}{C_s \rho \, d_i}. \tag{5}$$

where γ is the thermal coupling constant, C_s is the specific heat capacity, ρ the density of water and d_i the depth of box i. The restoring temperatures are fitting parameters. Note that the model in Fig. 2 is only valid for positive m_0 and m_1 and that the light blue arrow flips if $m_1 > m_0$. The salinity and temperature values in the box model are fitted to sea surface temperature data from the World Ocean Atlas (winter averages between 1971-2000) (Reagan et al., 2024). All stacked boxes add to depth of 3000m except for boxes 3 and 4 that add to 1500m because the Nordic Seas have a shallower average depth than the Atlantic. The regions for the Nordic Seas and the subpolar North Atlantic are shown in Fig. 1. Only the western Nordic Seas and
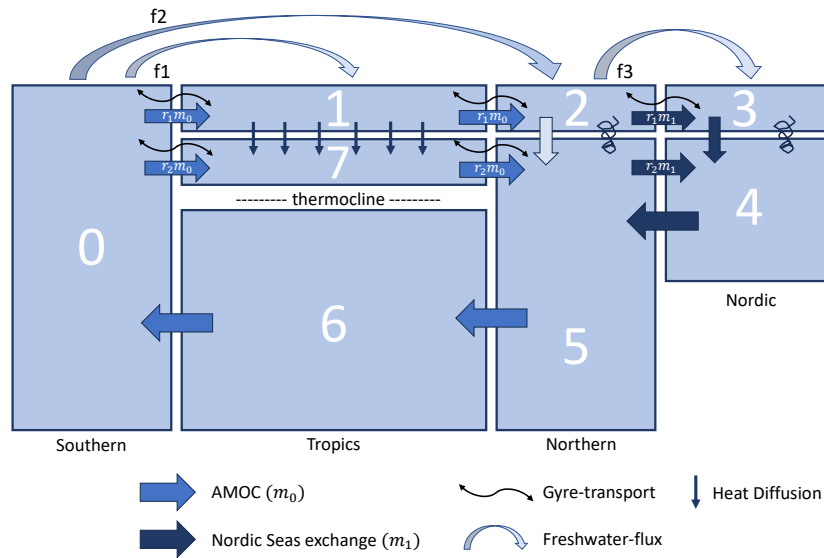
Figure 2. Schematic representation of the box model of the Atlantic Ocean. $f_1 - f_3$ are the freshwater fluxes between the boxes. The wavy arrows indicate gyre transport. The solid large arrows represent AMOC (medium blue) and NOC (dark blue) respectively, while the small solid arrows indicate diffusive heat transport. The coils mark convection.

the Labrador Sea are considered because this is where the main convection sites are located (Fig. 1). While the Labrador Sea dominates the contributions to the North Atlantic Deep Waters (Fröhle et al., 2022), the western Nordic Seas are also known to contribute significantly to the dense overflows that feed the lower limb of the AMOC (Huang et al., 2020; Brakstad et al.,

2023). Furthermore, most of the freshwater input in the northern Atlantic is being focused towards the Labrador Sea due to the counter clockwise rotation of the ocean currents around Greenland (Yang et al., 2016), which favours this region for hosing

150 experiments. Lastly, the water in the Labrador Sea is colder, which facilitates the onset of convection in the model. In the following we will refer to these regions simply as the Nordic Seas and northern Atlantic for simplicity.

We also implement a diffusion process between the tropical surface and intermediate waters to regulate the temperature in box 7.

155

The model equations for positive m_0 and m_1 as well as $m_0 > m_1$ are thus:

$$\frac{dT_0}{dt} = \lambda_0(T_0^* - T_0) + \frac{m_0}{V_0}(T_6 - T_0) + \frac{aK_s}{V_0}(T_1 - T_0) + \frac{bK_s}{V_0}(T_7 - T_0) \tag{6}$$

$$\frac{dT_1}{dt} = \lambda_1(T_1^* - T_1) + \frac{am_0}{V_1}(T_0 - T_1) + \frac{aK_s}{V_1}(T_0 - T_1) + \frac{aK_n}{V_1}(T_2 - T_1) + \frac{\eta}{V_1}(T_7 - T_1) \tag{7}$$

$$\frac{dT_2}{dt} = \lambda_2(T_2^* - T_2) + \frac{am_0}{V_2}(T_1 - T_2) + \frac{aK_n}{V_2}(T_1 - T_2) + \frac{aK_{nn}}{V_2}(T_3 - T_2) + \frac{c_0}{V_2}(T_5 - T_2) \tag{8}$$

160
$$\frac{dT_3}{dt} = \lambda_3(T_3^* - T_3) + \frac{am_1}{V_3}(T_2 - T_3) + \frac{aK_{nn}}{V_3}(T_2 - T_3) + \frac{c_1}{V_3}(T_4 - T_3) \tag{9}$$

$$\frac{dT_4}{dt} = \frac{am_1}{V_4}(T_3 - T_4) + \frac{bm_1}{V_4}(T_5 - T_4) + \frac{c_1}{V_4}(T_3 - T_4) \tag{10}$$

$$\frac{dT_5}{dt} = \frac{m_1}{V_5}(T_4 - T_5) + \frac{a(m_0 - m_1)}{V_5}(T_2 - T_5) + \frac{bm_0}{V_5}(T_7 - T_5) + \frac{bK_n}{V_5}(T_7 - T_5) + \frac{c_0}{V_5}(T_2 - T_5) \tag{11}$$

$$\frac{dT_6}{dt} = \frac{m_0}{V_6}(T_5 - T_6) \tag{12}$$

$$\frac{dT_7}{dt} = \frac{bm_0}{V_7}(T_0 - T_7) + \frac{bK_s}{V_7}(T_0 - T_7) + \frac{bK_n}{V_7}(T_5 - T_7)\frac{\eta}{V_7}(T_1 - T_7) \tag{13}$$

165

$$\frac{dS_0}{dt} = -\frac{S_0}{V_0}(h_2 + h_1) + \frac{m_0}{V_0}(S_6 - S_0) + \frac{aK_s}{V_0}(S_1 - S_0) + \frac{bK_s}{V_0}(S_7 - S_0) \tag{14}$$

$$\frac{dS_1}{dt} = \frac{S_0}{V_1}h_1 + \frac{am_0}{V_1}(S_0 - S_1) + \frac{aK_s}{V_1}(S_0 - S_1) + \frac{aK_n}{V_1}(S_2 - S_1) + \frac{\eta}{V_1}(S_7 - S_1) \tag{15}$$

$$\frac{dS_2}{dt} = \frac{S_0}{V_2}(h_2 - h_3) + \frac{am_0}{V_2}(S_1 - S_2) + \frac{aK_n}{V_2}(S_1 - S_2) + \frac{aK_{nn}}{V_2}(S_3 - S_2) \tag{16}$$

$$\frac{dS_3}{dt} = \frac{S_0}{V_3}h_3 + \frac{am_1}{V_3}(S_2 - S_3) + \frac{aK_{nn}}{V_3}(S_2 - S_3) \tag{17}$$

170
$$\frac{dS_4}{dt} = \frac{am_1}{V_4}(S_3 - S_4) + \frac{bm_1}{V_4}(S_5 - S_4) + \frac{c_1}{V_4}(S_3 - S_4) \tag{18}$$

$$\frac{dS_5}{dt} = \frac{c_0}{V_5}(S_2 - S_5) + \frac{m_1}{V_5}(S_4 - S_5) + \frac{bm_0}{V_5}(S_7 - S_5) + \frac{a(m_0 - m_1)}{V_5}(S_2 - S_5) + \frac{bK_n}{V_5}(S_7 - S_5) \tag{19}$$

$$\frac{dS_6}{dt} = \frac{m_0}{V_6}(S_5 - S_6) \tag{20}$$

$$\frac{dS_7}{dt} = \frac{bm_0}{V_7}(S_0 - S_7) + \frac{bK_n}{V_7}(T_5 - T_7) + \frac{bK_s}{V_7}(T_0 - T_7) + \frac{\eta}{V_7}(S_1 - S_7) \tag{21}$$

with

$$m_0 = k_0(r_2\rho(S_2,T_2) + r_5\rho(S_5,T_5) - \rho(S_0,T_0)) \tag{22}$$

$$m_1 = k_1(r_3\rho(S_3,T_3) + r_4\rho(S_4,T_4) - r_2\rho(S_2,T_2) - r_5\rho(S_5,T_5)) \tag{23}$$

and

$$a = \frac{D_1}{D_1 + D_7} \tag{24}$$

$$b = 1 - a \tag{25}$$

$$r_2 = \frac{D_2}{D_2 + D_5} \tag{26}$$

$$r_5 = 1 - r_2 \tag{27}$$

$$r_3 = \frac{D_3}{D_3 + D_4} \tag{28}$$

$$r_4 = 1 - r_3 \tag{29}$$

where D_i is the depth of box i. All surface boxes have a depth of 100 m. This depth is chosen according to the MLD in the Labrador Sea without convection (Gillard et al., 2022). The parameter c is either $>> m_0$ or 0 depending on whether or not the density stratification is stable. The exact value of c is not critical, as long as it is large enough to guarantee that the surface box and deep water box are sufficiently mixed. The parameters K_s, K_n and K_{nn} are constant and take into account the gyre transport between the respective boxes. The values of K_s and K_n are 3.4 Sv respectively and were estimated using the results of (Wood et al., 2019). The value of K_{nn} was chosen to be 1 Sv.

η is the heat diffusion constant. η, f_1, k_0, k_1 and the restoring temperatures are fitted by minimizing the loss function

$$l = \frac{1.7}{8}\sum_k (T_k - \overline{T}_k)^2 + \frac{7.9}{8}\sum_k (S_k - \overline{S}_k)^2 + (m_0 - \overline{m_0})^2 + (m_1 - \overline{m_1})^2 + 10(c_1 - \overline{c_1})^2 \tag{30}$$

where k is the box number and the overlined letters are the present day values according to WOA23 data and, in case of AMOC (m_0, 17 Sv) and NOC (m_1, 6 Sv), current meter observations (Wett et al., 2023; Hansen and Østerhus, 2000). The last term is added to guarantee convection in the Nordic Seas. The weights for the salinity and temperature differences are the values of α and β in the linear EOS. We divide by 8 to average over the 8 boxes.

A value of 0.07 Sv for f_2 is chosen according to (Yang et al., 2016). They mention 20-30 mSv precipitation in the northern Atlantic region and about 40 mSv of freshwater influx from Arctic Sea Ice, Greenland Ice Sheet and the Canadian Arctic Archipelago combined. f_3 is chosen to be smaller than but in the same order of magnitude as f_2 since in the model freshwater is transported directly from the northern Atlantic into the Nordic Seas. The data is averaged from 0m-100m for the surface layers and from 100m to a maximum depth of 3000m/1500m, according to the depth of the boxes.

The same data was used to calculate the order of magnitude of the increase in f_2 per year. An approximate increase rate
205   of 0.75 mSv/yr was obtained from (Yang et al., 2016) for the influx from the Arctic Sea Ice, Greenland Ice Sheet and the
Canadian Arctic Archipelago (calculated between 2000 and 2020). The net precipitation increased by a factor of three in about
25 years (Josey and Marsh, 2005), so about 8% per year. Multiplying this with the 20-30 mSv measured by (Yang et al., 2016)
one gets a crude estimate of the increase which is 2 mSv per year.

3   Results

210   ### 3.1   Increased Heat Flow Into the Nordic Seas in CM2.6 Simulations

Comparing the CM2.6 preindustrial control (PIC) and $2xCO_2$ simulations, we find a reduction of -0.09 PW in MHT into the
subpolar North Atlantic and the Labrador Sea following a doubling of atmospheric CO_2. In contrast to this reduced MHT into
the subpolar North Atlantic, there is an increase of 0.07 PW into the Nordic Seas over the same period. A heat budget analysis
further reveals that in $2xCO_2$, this divergence in MHT is balanced by a substantial reduction in surface heat flux (SHF) of -0.16
215   PW (SHF_{2xCO_2}-SHF_{PIC}) over the subpolar North Atlantic. A detailed presentation of the CM2.6 heat budget results is given
in table 1.

	PIC	$2xCO_2$	$2xCO_2$ - PIC
Subpolar North Atlantic			
MHT_{in}	0.6 PW	0.51 PW	-0.09 PW
SHF	0.42 PW	0.26 PW	-0.16 PW
Nordic Seas			
MHT_{in}	0.17 PW	0.24 PW	0.07 PW
SHF	0.17 PW	0.23 PW	0.06 PW

Table 1. Meridional heat transport into the subpolar North Atlantic and the Nordic Seas under PIC and 2xCO$_2$ Forcing. We present
the results from a subpolar North Atlantic and Nordic Seas heat budget analysis in both CM2.6 simulations. We calculate the heat inflow
(MHT_{in}) as well as the surface heat flux (SHF) of both regions and under both forcings. Changes in ocean heat content as a budget residual
are neglected. Furthermore, we show the changes of MHT_{in} and SHF when doubling the atmospheric CO_2 concentration in CM2.6.

3.1.1   Heat Flow Decomposition

Dynamic-Thermodynamic Decomposition To assess the drivers of MHT anomalies, we decompose them into dynamic, ther-
modynamic, and nonlinear contributions. This allows us to determine whether changes in MHT are primarily driven by changes
220   in the mass transport of the flow or its temperature under a two-fold CO_2 forcing. For the subpolar North Atlantic, dynamic

changes in ocean circulation contribute by -0.36 PW to the reduction, making them the dominant factor of the decline presented above. In contrast, thermodynamic effects play a lesser role, contributing only about a quarter of the dynamic component (-0.08 PW). This shows that the weakening of MHT at this latitude is primarily caused by changes in the mean flow ocean circulation rather than changes in temperature (see table 2). Results in the Nordic Seas are similar. The dynamic component remains
225   the primary driver (0.03 PW) of MHT', with its magnitude exceeding that of the thermodynamic contribution (0.01 PW, see table 2). Additionally, a strong non-linear term is present, reflecting the covariation of velocity and temperature anomalies representing the eddy-mediated heat transport. The results indicate that, analogous to the subpolar North Atlantic, variations in circulation patterns dominate the differences in MHT under PIC and 2xCO2 forcing in CM2.6. Hence, the findings imply an anticorrelation between AMOC and NOC-driven MHT changes under increased CO_2 forcing in CM2.6.

	Subpolar North Atlantic	Nordic Seas
$2xCO_2$ - PIC		
Thermodynamic	-0.08 PW	0.01 PW
Dynamic	-0.36 PW	0.03 PW
Nonlinear	0.35 PW	0.03 PW

Table 2. Results from the Dynamic-Thermodynamic-Decomposition of Meridional Heat Transport into the subpolar North Atlantic and the Nordic Seas. We present MHT anomalies when decomposed into thermodynamic, dynamic and non-linear contributions. The sum for each region matches the MHT changes presented in table 1.

230   **Overturning-Gyre Decomposition** To further investigate the mechanisms driving MHT anomalies, we decompose MHT into contributions from the wind-driven gyre circulation and the meridional overturning circulation (see Methods 2.3.2). Since this decomposition focuses on total MHT, we first examine the dominant contributors to northward heat transport into the subpolar North Atlantic and the Nordic Seas before evaluating how changes in these components drive MHT anomalies under increased CO_2 forcing in CM2.6. The results are summarized in table 3. For the subpolar North Atlantic, the decomposition reveals that
235   MHT is primarily driven by the overturning circulation. In both simulations, the MOC component dominates, accounting for 86% of MHT in the PIC run and increasing to 91% under $2xCO_2$ forcing (see table 3).

Investigating changes to MHT entering the subpolar North Atlantic under increased CO_2 forcing, the MOC component accounts for 57.5% of the total MHT anomalies, indicating that the weakening of the overturning circulation is the dominant factor in the detected reduction in CM2.6. However, the gyre component also contributes to the reduction, accounting for
240   42.5% of MHT anomalies. For the Nordic Seas, the decomposition of MHT anomalies reveals that the changes in MHT due to increased atmospheric CO_2 forcing are primarily driven by changes in the MOC component. The gyre contribution exhibits a slight weakening effect on MHT', but its influence is minor compared to the dominant MOC-driven increase (see table 3).

	Subpolar North Atlantic	Nordic Seas
PIC		
MOC Component	0.51 PW	-0.13 PW
Gyre Component	0.09 PW	0.3 PW
$2xCO_2$		
MOC Component	0.46 PW	-0.03 PW
Gyre Component	0.05 PW	0.27 PW
$2xCO_2$ - PIC		
MOC Component	-0.05 PW	0.1 PW
Gyre Component	-0.04 PW	-0.03 PW

Table 3. Results from the Overturning-Gyre-Decomposition of Meridional Heat Transport into the subpolar North Atlantic and the Nordic Seas. We present MHT estimates from the PIC simulation as well as the $2xCO_2$ simulation in CM2.6 decomposed into contributions from MOC and the gyre circulation. Contributions to MHT anomalies when increasing the atmospheric CO_2 concentration in CM2.6 are given as well.

3.2 Box Model Results

In the previous section it was shown that the increased heat transport into the Nordic Seas in 2xCO2 simulations with GFDL CM2.6 is associated with a strengthening of Nordic Overturning. In the following, we will use our box model to conceptually explore the possible reasons behind this increase by doing hosing and global warming experiments under the assumption that both, AMOC and NOC, are driven by density gradients. We compared different hosing rates ranging from 2 mSv/year to 4 mSv/year and global warming scenarios from $0.1°$C/decade to $0.4°$C/decade. We combined each hosing rate with each global warming scenario. The results are shown in Fig. 3. The warming was imposed on the restoring temperatures T^*.

The AMOC exhibits a non-linear response to freshwater hosing (Fig. 3 (a), (c), (e)). The hosing rate determines the steepness of the trajectory while the imposed warming accelerates convection shutdown due to decreasing surface buoyancy. Under 2mSv/year of hosing and 0.1 °C/decade warming, convection ceases around year 2155 followed by a steep AMOC decline and final shutdown around 2170. For a warming rate of 0.4 °C/decade, however, convection already stops around 2130 - several decades earlier.

The increase in NOC as a response to a weakening AMOC is clearly visible in the box model and limited to about 1 Sv over 100 years (Fig. 3 (f)), equivalent to a rate of 0.1 Sv per decade. This order of magnitude agrees well with climate model projections (Årthun et al., 2023). Even though the hosing still appears to be the dominant factor, the warming steepens the
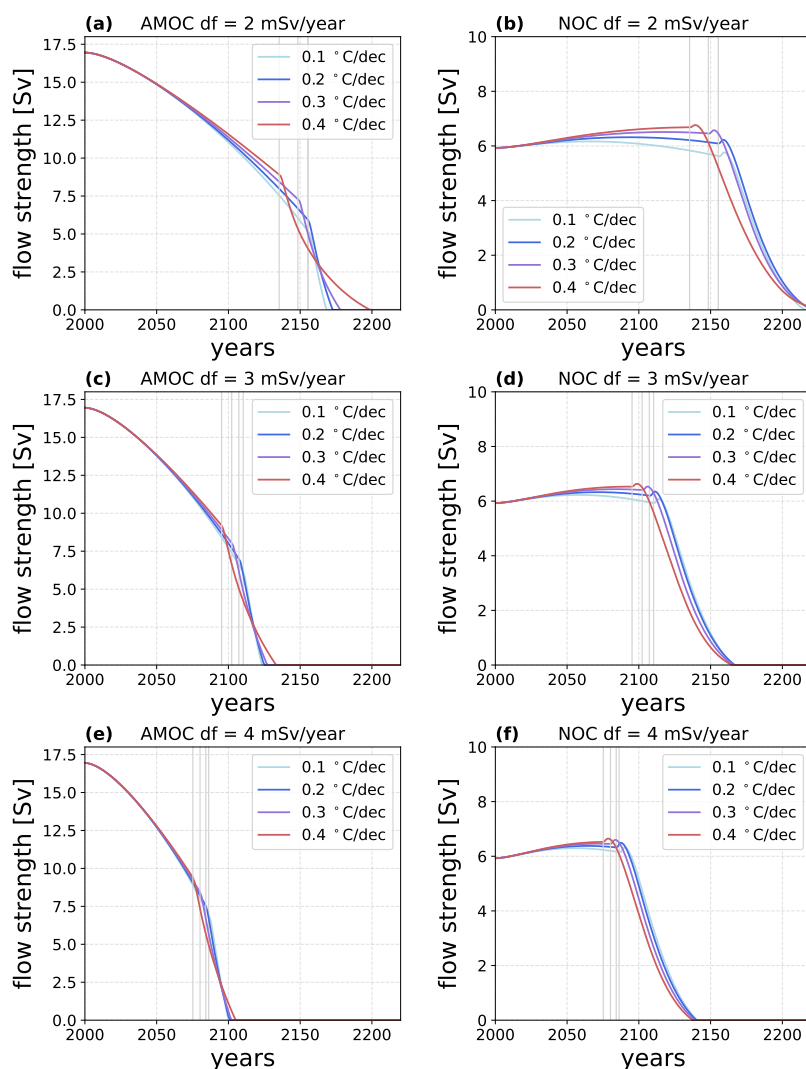
Figure 3. Comparison of AMOC and NOC hysteresis for different hosing rates and global warming scenarios in the box model. Grey lines represent the time of convection shut down in the northern Atlantic (AMOC) and Nordic Seas (NOC).

260 NOC's trajectory, due to the temperature difference between the northern Atlantic and the Nordic Seas. Warming impacts the density in the northern Atlantic more than in the Nordic Seas because of the nonlinearity in the equation of state, thus increas-

ing the density gradient between the two ocean basins.

Due to the weakening of the AMOC, more freshwater accumulates in the northern Atlantic (salt advection feedback), de-
265 creasing the surface density and continuing to steepen the density gradient between the Nordic Seas and the northern Atlantic.
This in turn increases exchange between the northern Atlantic and Nordic Seas, causing the NOC to increase. This anticorre-
lation only breaks down when convection in the northern Atlantic shuts off because the freshwater at the surface layer can no
longer be mixed downward at a sufficient rate. This causes more freshwater to be transported into the Nordic Seas via gyre
transport and increased NOC, shutting down Nordic Sea convection in turn. This marks the crossing of the NOC's tipping
270 point, which is followed by a steep decline in overturning strength. Additionally, we find that the decline of the AMOC is
mitigated by an increase in NOC, as more cold, dense water is supplied to the northern Atlantic, counteracting the decrease in
density.

To decompose the response of AMOC and NOC to the combined forcing, we conducted experiments with isolated global
warming and hosing scenarios (Fig. 4). Under isolated global warming the AMOC initially stays stable, while the NOC shows
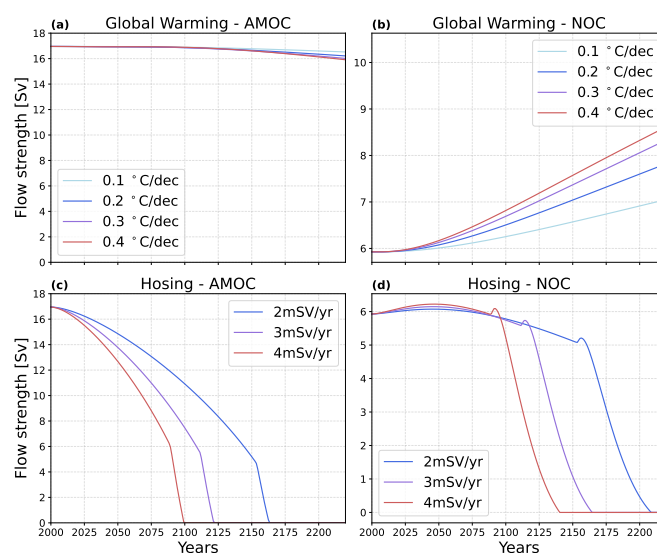
Figure 4. (a) AMOC under global warming (b) NOC under global warming (c) AMOC under hosing (d) NOC under hosing
275

an accelerating increase until 2050 after which the rate of increase stays constant. The temperature difference between the
northern Atlantic and the Southern Ocean is not as large as between the northern Atlantic and Nordic Seas, which explains the
weak change in AMOC strength, since the thermal expansion coefficient is similar in both boxes.

280 Under hosing, the AMOC decreases steeply, while the NOC shows an increase in the short-term response due to the same

mechanisms explained above, and then begins to decline around 2050 until convection shuts off and both currents cease. The decrease in NOC under isolated hosing, is explained by the continuous freshwater transport into the Nordic Seas via gyre transport and increased NOC which weakens the density gradient between the subpolar North Atlantic and Nordic Seas.

285   These results imply a short-term and long-term response under combined forcing: The short-term response of the current system is characterised by a negative feedback loop: Hosing weakens the AMOC by decreasing the water density in the northern Atlantic. This, in turn, increases the NOC and thus the transport of cold, dense water into the northern Atlantic which mitigates the AMOC's decline, but does not prevent it.

290   In the long term, warming prevents the decline of the NOC (Fig.4(b)), but accelerates the breakdown of convection(Fig.3) which causes an earlier AMOC shut-down. For very high hosing rates, the distances between the break-off points begin to diminish. This is because the accumulation of freshwater is so strong that it outweighs the effect of increasing temperature (Fig. 3).

295   In order to compare with the box model results, we analyse density changes between the two forcing scenarios in CM2.6. The results in Figure 5 support the findings of the box model by illustrating how the density gradients between the northern Atlantic and the Nordic Seas strengthen under elevated CO_2 concentrations. The subpolar North Atlantic exhibits a pronounced density decrease, while the Nordic Seas show a localized density increase, particularly along the Greenland–Scotland Ridge and the western Nordic Seas. This pattern indicates that warming and freshening in the subpolar North Atlantic under increased 300 CO_2 reduce surface density there, whereas the Nordic Seas experience comparatively smaller density reductions or even densification, consistent with the nonlinear thermal response in the equation of state discussed earlier. The resulting enhanced meridional density gradient aligns with the box model mechanism, where a weakening AMOC and surface buoyancy changes drive increased Nordic Overturning (NOC). A latitude–depth cross-section of the red box in Fig. 5(a), further highlights this contrast: the upper ocean in the Labrador Sea becomes significantly lighter, while the intermediate and deep layers toward 305 the Nordic Seas show minor density increases, pointing to shoaling of isopycnals in the subpolar region and deepening in the Nordic Seas. Together, these patterns confirm that under increased CO_2, density-driven contrasts between the two basins intensify, as the box model predicts.

4   Discussion

Our results showing a stable or slightly increasing NOC under warming conditions appear to be in agreement with observational 310   data (Chafik et al., 2025; Larsen et al., 2024), alongside a future increase in NOC predicted in GCMs (Årthun et al., 2023). The density decline in the subpolar gyre in the CM2.6 model and the box model is consistent with the declining density since 1950 found there in observed data (Chafik et al., 2022), as well as with the fact that salinity there is now at its lowest in 120 years of measurements (Holliday et al., 2020). Li and Liu (2025) compare CMIP ensembles with and without a weakened AMOC
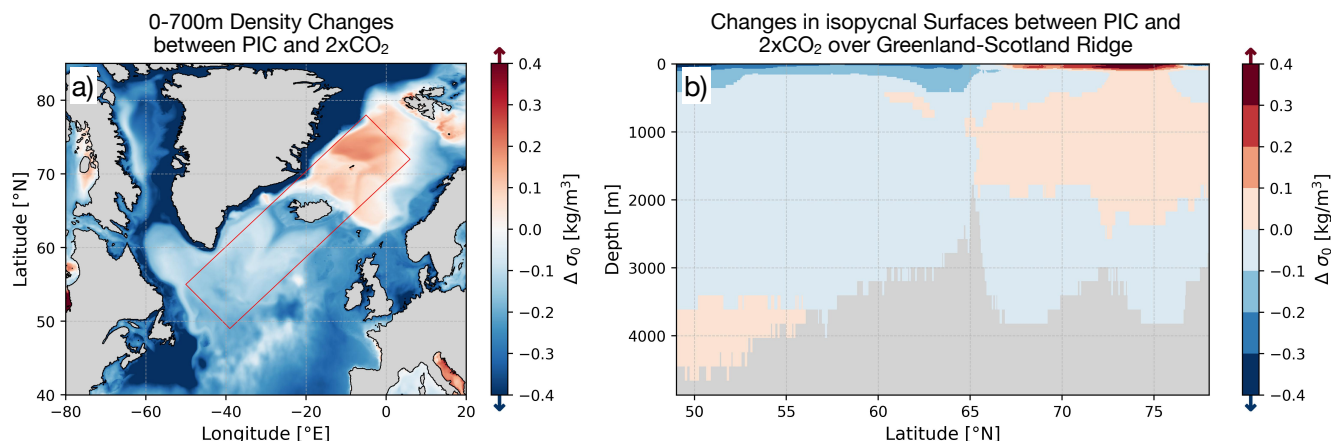
Figure 5. Density changes under elevated atmospheric CO_2 concentration averaged over 20 model years. **a)** is depicting density changes in the upper 700 m between the CM2.6 PIC run and the $2xCO_2$ scenario. **b)** is showing the latitude-depth cross section of the red box in **a)**.

and find that the warming in the Nordic Seas is directly correlated with a weaker AMOC state. Our results indicate that the
315   reason for this correlation is an increase in the meridional density gradient between the northern Atlantic and the Nordic Seas.
In CM2.6 we observe an increase in heat transport towards the Nordic seas and the steepening of the North Atlantic-Nordic
Seas density gradient. This is in line with the findings of Keil et al. (2020) who identified increased heat transport towards the
Nordic Seas as one of the drivers of the North Atlantic Warming Hole. Future work should investigate whether these results
are consistent across different models.

320

Simple conceptual box models are not intended for quantitative predictions but rather to qualitatively examine basic physi-
cal mechanisms. The box model used in this study is simplified and several factors that contribute to the behaviour of the
AMOC, Nordic Overturning, and convection, are not considered here. For example, the model lacks variations in surface heat
and moisture fluxes due to both the seasonal cycle and internal climate variability even though both are important for the con-
325   vective process. If convection is e.g. shut off due to increased surface heating, fresh water can accumulate at the convection
site, inhibiting the re-initiation of deep mixing (Kuhlbrodt et al., 2001).

Another limitation of the box model is the way in which convection is parametrised. While the strength of convection scales
with the temperature gradient between the surface and the deep water, it changes the temperature of the entire box, when in re-
330   ality convection is localised and can vary in depth. The model can therefore not accurately represent how much exchange takes
place between the surface and the deep water, potentially affecting the density gradient between the North Atlantic and Nordic
Seas. The lack of localised convection might also lead to a premature shutdown of convection in our model: Once the surface
water is lighter than the deep water, convection switches off. In reality, however, e.g. winds might trigger localised convection

events that mix freshwater into the deep ocean and thus mitigate the surface freshening. Additionally, the gyre strengths in this
model are constant as is the surface layer depth, which is of course not the case in the real world. Given that the gyre transport
exhibits substantial decadal variability (Böning et al., 2006), and that its magnitude influences water-mass exchange between
and transformation within the boxes (e.g. Årthun et al. (2023)), both the strength of the AMOC and the timing of convection
shutdown may be affected by this variability, which is itself modulated by the North Atlantic Oscillation (NAO) (Böning et al.,
2006). Potential impacts of AMOC/NOC changes on the NAO, and consequently the gyre transport are not accounted for in
this analysis. Nevertheless, such feedbacks would likely not impact the link between AMOC and NOC dsicussed here.

The box model also assumes fixed domains (regions), implying that convection and overturning are not allowed to move
geographically. It has, for example, been shown that reduced overturning in the Nordic Seas can be compensated by increased
overturning in the Arctic Ocean (Bretones et al., 2022; Årthun et al., 2025). This process could add resilience to the northern
overturning circulation, but would, however, likely not alter the fundamental mechanism discussed here (i.e., the link between
AMOC and NOC) in the long term.

Finally, our box model does not consider other ocean basins. While it has been shown by Wood et al. (2019) that the hos-
ing rate needed to switch off the AMOC is sensitive to the gyre transport from the Indo-Pacific thermocline into the Southern
Ocean, this does not impact the fundamental relationship between the AMOC and NOC we describe in our results, only
potentially impacting where the tipping point due to hosing lies.

5 Conclusions

This study aims to investigate the increase of heat transport into the Nordic Seas and overturning, and its possible connection
to a weakening AMOC under global warming conditions. Results from the high resolution climate model CM2.6 suggest that
the surface cooling in northern Atlantic is primarily caused by a weakening of the AMOC and an associated reduction in
northward heat transport. However, overturning in the Nordic Seas also transports more heat northward, driving positive SST
anomalies there. Our box model suggests that this increase in OHT into the Nordic Seas is driven by increased Nordic over-
turning linked to the weakening of the AMOC. We compare different hosing rates ranging from 2 mSv/year to 5 mSv/year and
global warming scenarios from 0.1 °C/decade to 0.4 °C/decade, both separately and in combination, to investigate the impact
of increased freshwater forcing and global warming on the AMOC-NOC current system. When combined, the stability of the
system is determined primarily by the freshwater flux, with the temperature forcing determining only the timing of the tipping.
In the first 50 years, the increased freshwater input weakens the AMOC, leading to freshwater accumulation in the northern
Atlantic and an increase in the density gradient between the Nordic Seas and the northern Atlantic, strengthening the NOC. In
the long-term (> 50 years), the NOC might continue to strengthen (Fig. 3) because the response to an increase in temperature
(Fig. 4(b)) counteracts the weakening of the NOC by freshening of the Nordic Seas due to gyre transport and enhanced NOC
(Fig. 4(c)). The anticorrelation between AMOC and NOC only stops when convection breaks down (Fig. 3), leading to rapid

freshwater accumulation in both ocean surfaces and thus to a breakdown of AMOC and NOC.

In summary, we propose a mechanism that links the strength and stability of NOC and AMOC via the density gradient be-
370 tween the subpolar North Atlantic and Nordic seas. Initially, the NOC strengthens driven by an increased meridional density
gradient due to warming and a freshening of the northern Atlantic caused by an AMOC slow-down until both currents collapse
following the shutdown of convection. The stronger NOC causes an enhanced heat transport into the Nordic Seas, which po-
tentially explains the positive Nordic Seas SST trend observed over the last century by e.g. Caesar et al. (2018). This implies
that the future increase in Nordic Overturning might be a direct effect of the AMOC weakening and that the AMOC-NOC
375 system could potentially be steering towards a shutdown of convection.

Code and data availability. The code for the box model, figures 1, 3 & 4, as well as for the spatial averaging (including all data) is
available under: https://github.com/sasharoewer/AMOC-NOC-BOX-MODEL.git. The utilised CM2.6 model output is available from L.F.
(lukas.fiedler@uni-hamburg.de) upon reasonable request. Scripts for analysing CM2.6 model output are available from L.F. (lukas.fiedler@uni-
hamburg.de) upon reasonable request.

380 *Author contributions.* Sasha R. conducted the box model simulation and analysis and wrote the manuscript with help from all co-authors.
L.F. conducted the CMIP2.6 heat transport analysis and wrote the pursuant results. M.Å. contributed knowledge on the Nordic Seas and
wrote a part of the introduction, also contributing to the refinement of the manuscript. W.H. helped refine and structure the manuscript.
Stefan R. conceived of and supervised the project, also contributing to the analysis of the heat transport and box model results, and writing
of the manuscript.

385 *Competing interests.* The authors declare that they have no conflict of interest.

Acknowledgements. Willem Huiskamp is part of PIK's Planetary Boundaries Science Lab and is funded by Virgin Unite. Marius Årtun was
funded by the Research Council of Norway project Overturning circulation in the new Arctic (Grant 335255). The Authors acknowledge the
generosity of NOAA/GFDL in supplying the CM2.6 model output.

References

390 Årthun, M., Asbjørnsen, H., Chafik, L., Johnson, H. L., and Våge, K.: Future strengthening of the Nordic Seas overturning circulation, Nature Communications, 14, 2065, https://doi.org/10.1038/s41467-023-37846-6, 2023.

Bony, S., Dufresne, J.-L., Treut, H. L., Morcrette, J.-J., and Senior, C.: On dynamic and thermodynamic components of cloud changes, Climate Dynamics, 22, 71–86, https://doi.org/10.1007/s00382-003-0369-6, 2004.

Bosse, A., Fer, I., Søiland, H., and Rossby, T.: Atlantic water transformation along its poleward pathway across the Nordic Seas, Journal of
395 Geophysical Research: Oceans, 123, 6428–6448, https://doi.org/10.1029/2018JC014147, 2018.

Brakstad, A., Gebbie, G., Våge, K., Jeansson, E., and Ólafsdóttir, S. R.: Formation and pathways of dense water in the Nordic Seas based on a regional inversion, Progress in Oceanography, 212, 102 981, https://doi.org/https://doi.org/10.1016/j.pocean.2023.102981, 2023.

Bretones, A., Nisancioglu, K. H., Jensen, M. F., Brakstad, A., and Yang, S.: Transient Increase in Arctic Deep-Water Formation and Ocean Circulation under Sea Ice Retreat, Journal of Climate, 35, 109 – 124, https://doi.org/10.1175/JCLI-D-21-0152.1, 2022.

400 Bryan, K.: Poleward Heat Transport by the Ocean: Observations and Models, Annual Review of Earth and Planetary Sciences, 10, 15–38, https://doi.org/10.1146/annurev.ea.10.050182.000311, 1982.

Bryden, H. L. and Imawaki, S.: Ocean heat transport, International Geophysics, 77, 455–474, 2001.

Böning, C. W., Scheinert, M., Dengg, J., Biastoch, A., and Funk, A.: Decadal variability of subpolar gyre transport and its reverberation in the North Atlantic overturning, Geophysical Research Letters, 33, https://doi.org/https://doi.org/10.1029/2006GL026906, 2006.

405 Caesar, L., Rahmstorf, S., Robinson, A., Feulner, G., and Saba, V.: Observed fingerprint of a weakening Atlantic Ocean overturning circulation, Nature, 556, 191–196, https://doi.org/https://doi.org/10.1038/s41586-018-0006-5, 2018.

Caesar, L., McCarthy, G. D., Thornalley, D. J. R., Cahill, N., and Rahmstorf, S.: Current Atlantic Meridional Overturning Circulation Weakest in Last Millennium, Nature Geoscience, 14, 118–120, https://doi.org/10.1038/s41561-021-00699-z, 2021.

Chafik, L., Holliday, N. P., Bacon, S., and Rossby, T.: Irminger Sea Is the Center of Action for Subpolar AMOC Variability, Geophysical
410 Research Letters, 49, https://doi.org/10.1029/2022GL099133, 2022.

Chafik, L., Årthun, M., Langehaug, H. R., et al.: The Nordic Seas overturning is modulated by northward-propagating thermohaline anomalies, Communications Earth & Environment, 6, 573, https://doi.org/10.1038/s43247-025-02557-x, 2025.

Chemke, R., Zanna, L., and Polvani, L. M.: Identifying a Human Signal in the North Atlantic Warming Hole, Nature Communications, 11, 1540, https://doi.org/10.1038/s41467-020-15285-x, 2020.

415 Copernicus Climate Change Service: ORAS5 global ocean reanalysis monthly data from 1958 to present, Copernicus Climate Change Service (C3S) Climate Data Store (CDS), https://doi.org/10.24381/cds.67e8eeb7, accessed on 03-11-2025, 2021.

Dagan, G., Stier, P., and Watson-Parris, D.: Aerosol Forcing Masks and Delays the Formation of the North Atlantic Warming Hole by Three Decades, Geophysical Research Letters, 47, e2020GL090 778, https://doi.org/10.1029/2020GL090778, 2020.

Decuypère, M., Tremblay, L. B., and Dufour, C. O.: Impact of Ocean Heat transport on Arctic Sea Ice variability in the GFDL CM2-O model
420 suite, Journal of Geophysical Research: Oceans, 127, e2021JC017 762, https://doi.org/https://doi.org/10.1029/2021JC017762, 2022.

Delworth, T. L., Rosati, A., Anderson, W., Adcroft, A. J., Balaji, V., Benson, R., Dixon, K., Griffies, S. M., Lee, H.-C., Pacanowski, R. C., et al.: Simulated climate and climate change in the GFDL CM2. 5 high-resolution coupled climate model, Journal of Climate, 25, 2755–2781, https://doi.org/https://doi.org/10.1175/JCLI-D-11-00316.1, 2012.

Diamond, R., Sime, L. C., Schroeder, D., Jackson, L. C., Holland, P. R., Alastrué de Asenjo, E., Bellomo, K., Danabasoglu, G., Hu,
425 A., Jungclaus, J., Montoya, M., Meccia, V. L., Saenko, O. A., and Swingedouw, D.: A weakened AMOC could cause Southern

Ocean temperature and sea-ice change on multidecadal timescales, Journal of Geophysical Research: Oceans, 130, e2024JC022 027, https://doi.org/10.1029/2024JC022027, 2025.

Dickson, R. R. and Brown, J.: The production of North Atlantic Deep Water: Sources, rates, and pathways, Journal of Geophysical Research: Oceans, 99, 12 319–12 341, https://doi.org/10.1029/94JC00530, 1994.

430   Dima, M. and Lohmann, G.: Evidence for Two Distinct Modes of Large-Scale Ocean Circulation Changes over the Last Century, Journal of Climate, 23, 5 – 16, https://doi.org/10.1175/2009JCLI2867.1, 2010.

Drijfhout, S., van Oldenborgh, G. J., and Cimatoribus, A.: Is a Decline of AMOC Causing the Warming Hole above the North Atlantic in Observed and Modeled Warming Patterns?, Journal of Climate, 25, 8373–8379, https://doi.org/https://doi.org/10.1175/JCLI-D-12-00490.1, 2012.

435   Drijfhout, S., Angevaare, J. R., Mecking, J., van Westen, R. M., and Rahmstorf, S.: Shutdown of northern Atlantic overturning after 2100 following deep mixing collapse in CMIP6 projections, Environmental Research Letters, 20, 094 062, https://doi.org/10.1088/1748-9326/adfa3b, 2025.

Dörr, J., Årthun, M., Eldevik, T., and Sandø, A. B.: Expanding influence of Atlantic and Pacific Ocean heat transport on winter sea-ice variability in a warming Arctic, Journal of Geophysical Research: Oceans, 129, e2023JC019 900, https://doi.org/10.1029/2023JC019900, 440   2024.

Fröhle, J., Handmann, P. V. K., and Biastoch, A.: Major sources of North Atlantic Deep Water in the subpolar North Atlantic from Lagrangian analyses in an eddy-rich ocean model, Ocean Sci., 18, 1431–1450, https://doi.org/10.5194/os-18-1431-2022, 2022.

Gillard, L. C., Pennelly, C., Johnson, H. L., and Myers, P. G.: The Effects of Atmospheric and Lateral Buoyancy Fluxes on Labrador Sea Mixed Layer Depth, Ocean Modelling, 171, 101 974, https://doi.org/https://doi.org/10.1016/j.ocemod.2022.101974, 2022.

445   Gregory, J. M., Dixon, K. W., Stouffer, R. J., Weaver, A. J., Driesschaert, E., Eby, M., Fichefet, T., Hasumi, H., Hu, A., Jungclaus, J. H., Kamenkovich, I. V., Levermann, A., Montoya, M., Murakami, S., Nawrath, S., Oka, A., Sokolov, A. P., and Thorpe, R. B.: A model intercomparison of changes in the Atlantic thermohaline circulation in response to increasing atmospheric CO2 concentration, Geophysical Research Letters, 32, https://doi.org/https://doi.org/10.1029/2005GL023209, 2005.

Griffies, S. M., Winton, M., Anderson, W. G., Benson, R., Delworth, T. L., Dufour, C. O., Dunne, J. P., Goddard, P., Morrison, A. K., Rosati, 450   A., et al.: Impacts on ocean heat from transient mesoscale eddies in a hierarchy of climate models, Journal of Climate, 28, 952–977, https://doi.org/https://doi.org/10.1175/JCLI-D-14-00353.1, 2015.

Hansen, B. and Østerhus, S.: North Atlantic–Nordic Seas exchanges, Progress in Oceanography, 45, 109–208, 2000.

Holliday, N. P., Bersch, M., Berx, B., et al.: Ocean Circulation Causes the Largest Freshening Event for 120 Years in Eastern Subpolar North Atlantic, Nature Communications, 11, 585, https://doi.org/10.1038/s41467-020-14474-y, 2020.

455   Huang, J., Pickart, R. S., Huang, R. X., Lin, P., Brakstad, A., and Xu, F.: Sources and upstream pathways of the densest overflow water in the Nordic Seas, Nature Communications, 11, 5389, https://doi.org/10.1038/s41467-020-19143-8, 2020.

Jackson, L. C., Kahana, R., Graham, T., Ringer, M., A., Woollings, T., Mecking, J. V., and Wood, R., A.: Global and European climate impacts of a slowdown of the AMOC in a high resolution GCM, Climate Dynamics, 45, 3299–3316, https://doi.org/https://doi.org/10.1007/s00382-015-2540-2, 2015.

460   Jackson, L. C., Alastrué de Asenjo, E., Bellomo, K., Danabasoglu, G., Haak, H., Hu, A., Jungclaus, J., Lee, W., Meccia, V. L., Saenko, O., Shao, A., and Swingedouw, D.: Understanding AMOC stability: the North Atlantic Hosing Model Intercomparison Project, Geoscientific Model Development, 16, 1975–1995, https://doi.org/10.5194/gmd-16-1975-2023, 2023.

Josey, S. A. and Marsh, R.: Surface freshwater flux variability and recent freshening of the North Atlantic in the eastern subpolar gyre, Journal of Geophysical Research: Oceans, 110, https://doi.org/https://doi.org/10.1029/2004JC002521, 2005.

465 Keil, P., Mauritsen, T., Jungclaus, J., et al.: Multiple Drivers of the North Atlantic Warming Hole, Nature Climate Change, 10, 667–671, https://doi.org/10.1038/s41558-020-0819-8, 2020.

Kuhlbrodt, T., Titz, S., Feudel, U., et al.: A simple model of seasonal open ocean convection, Ocean Dynamics, 52, 36–49, https://doi.org/10.1007/s10236-001-8175-3, 2001.

Kuhlbrodt, T., Griesel, A., Montoya, M., Levermann, A., Hofmann, M., and Rahmstorf, S.: On the driving processes of the Atlantic meridional
470 overturning circulation, Reviews of Geophysics, 45, https://doi.org/https://doi.org/10.1029/2004RG000166, 2007.

Larsen, K. M. H., Hansen, B., Hátún, H., Johansen, G. E., Østerhus, S., and Olsen, S. M.: The Coldest and Densest Over-flow Branch Into the North Atlantic is Stable in Transport, But Warming, Geophysical Research Letters, 51, e2024GL110097, https://doi.org/https://doi.org/10.1029/2024GL110097, e2024GL110097 2024GL110097, 2024.

Levermann, A., Griesel, A., Hofmann, M., Montoya, M., and Rahmstorf, S.: Dynamic sea level changes following changes in the thermoha-
475 line circulation, Climate Dynamics, 24, 347–354, 2005.

Li, K. Y. and Liu, W.: Weakened Atlantic Meridional Overturning Circulation Causes the Historical North Atlantic Warming Hole, Communications Earth & Environment, 6, 416, https://doi.org/10.1038/s43247-025-02403-0, 2025.

Marshall, J. and Schott, F.: Open-ocean convection: Observations, theory and models, Reviews of Geophysics, 37, 1–64, https://doi.org/10.1029/98RG02739, 1999.

480 Mauritzen, C.: Production of dense overflow waters feeding the North Atlantic across the Greenland–Scotland Ridge. Part 1: Evidence for a revised circulation scheme, Deep Sea Research Part I: Oceanographic Research Papers, 43, 769–806, https://doi.org/10.1016/0967-0637(96)00037-4, 1996.

Nycander, J., Hieronymus, M., and Roquet, F.: The nonlinear equation of state of sea water and the global water mass distribution, Geophysical Research Letters, 42, 7714–7721, https://doi.org/https://doi.org/10.1002/2015GL065525, 2015.

485 Oldenburg, D., Armour, K. C., Thompson, L., and Bitz, C. M.: Distinct Mechanisms of Ocean Heat Transport Into the Arctic Under Internal Variability and Climate Change, Geophysical Research Letters, 45, 7692–7700, https://doi.org/10.1029/2018gl078719, 2018.

Olsen, S., Hansen, B., Quadfasel, D., et al.: Observed and modelled stability of overflow across the Greenland–Scotland ridge, Nature, 455, 519–522, https://doi.org/10.1038/nature07302, 2008.

Orihuela-Pinto, B., England, M. H., and Taschetto, A. S.: Interbasin and interhemispheric impacts of a collapsed Atlantic Overturning
490 Circulation, Nature Climate Change, 12, 558–565, https://doi.org/https://doi.org/10.1038/s41558-022-01380-y, 2022.

Pickart, R. S., Spall, M. A., Ribergaard, M. H., Moore, G. W. K., and Milliff, R. F.: Deep convection in the Irminger Sea forced by the Greenland tip jet, Nature, 424, 152–156, https://doi.org/10.1038/nature01729, 2003.

Qasmi, S.: Past and Future Response of the North Atlantic Warming Hole to Anthropogenic Forcing, Earth System Dynamics, 14, 685–695, https://doi.org/10.5194/esd-14-685-2023, 2023.

495 Reagan, J. R., Boyer, T. P., García, H. E., Locarnini, R. A., Baranova, O. K., Bouchard, C., Cross, S. L., Mishonov, A. V., Paver, C. R., Seidov, D., Wang, Z., and Dukhovskoy, D.: World Ocean Atlas 2023, https://www.ncei.noaa.gov/products/world-ocean-atlas, dataset: NCEI Accession 0270533, 2024.

Ren, Q., Xie, S. P., Peng, Q., et al.: Equatorial Atlantic mid-depth warming indicates Atlantic meridional overturning circulation slowdown, Communications Earth & Environment, 6, 819, https://doi.org/10.1038/s43247-025-02793-1, 2025.

500   Roach, A., Aagaard, K., and Carsey, F.: Coupled ice-ocean variability in the Greenland Sea, Atmosphere-Ocean, 31, 319–337, https://doi.org/10.1080/07055900.1993.9649474, 1993.

Rudels, B.: Haline convection in the Greenland Sea, Deep Sea Research Part A: Oceanographic Research Papers, 37, 1491–1511, https://doi.org/10.1016/0198-0149(90)90141-H, 1990.

Saba, V. S., Griffies, S. M., Anderson, W. G., Winton, M., Alexander, M. A., Delworth, T. L., Hare, J. A., Harrison, M. J., Rosati, A., Vecchi,

505   G. A., et al.: Enhanced warming of the N orthwest A tlantic O cean under climate change, Journal of Geophysical Research: Oceans, 121, 118–132, https://doi.org/https://doi.org/10.1002/2015JC011346, 2016.

Shu, Q. et al.: Arctic Ocean Amplification in a warming climate in CMIP6 models, Science Advances, 8, eabn9755, https://doi.org/10.1126/sciadv.abn9755, 2022.

Steele, M., Morley, R., and Ermold, W.: PHC: A global ocean hydrography with a high-quality Arctic Ocean, Journal of Climate, 14, 2079–

510   2087, https://doi.org/https://doi.org/10.1175/1520-0442(2001)014<2079:PAGOHW>2.0.CO;2, 2001.

Stouffer, R. J., Yin, J., Gregory, J. M., Dixon, K. W., Spelman, M. J., Hurlin, W., Weaver, A. J., Eby, M., Flato, G. M., Hasumi, H., Hu, A., Jungclaus, J. H., Kamenkovich, I. V., Levermann, A., Montoya, M., Murakami, S., Nawrath, S., Oka, A., Peltier, W. R., Robitaille, D. Y., Sokolov, A., Vettoretti, G., and Weber, S. L.: Investigating the Causes of the Response of the Thermohaline Circulation to Past and Future Climate Changes, Journal of Climate, 19, 1365 – 1387, https://doi.org/10.1175/JCLI3689.1, 2006.

515   Trenberth, K. E. and Fasullo, J. T.: Atlantic meridional heat transports computed from balancing Earth's energy locally, Geophysical Research Letters, 44, 1919–1927, https://doi.org/10.1002/2016GL072475, 2017.

van Westen, R. M., den Toom, M., and Dijkstra, H. A.: Physics-based early warning signal shows that AMOC is on tipping course, Science Advances, 10, eadk1189, https://doi.org/10.1126/sciadv.adk1189, 2024.

van Westen, R. M., Kliphuis, M., and Dijkstra, H. A.: Collapse of the Atlantic Meridional Overturning Circulation in a Strongly Eddying

520   Ocean-Only Model, Geophysical Research Letters, 52, e2024GL114 532, https://doi.org/10.1029/2024GL114532, 2025a.

van Westen, R. M., van der Wiel, K., Falkena, S. K. J., and Selten, F.: Changing European hydroclimate under a collapsed AMOC in the Community Earth System Model, Hydrology and Earth System Sciences, 29, 6607–6630, https://doi.org/10.5194/hess-29-6607-2025, 2025b.

Vellinga, M. and Wood, R. A.: Global Climatic Impacts of a Collapse of the Atlantic Thermohaline Circulation, Climatic Change, 54,

525   251–267, https://doi.org/10.1023/A:1016168827653, 2002.

Weaver, A. J., Eby, M., Kienast, M., and Saenko, O. A.: Response of the Atlantic meridional overturning circulation to increasing atmospheric CO2: Sensitivity to mean climate state, Geophysical Research Letters, 34, https://doi.org/https://doi.org/10.1029/2006GL028756, 2007.

Weijer, W., Cheng, W., Garuba, O. A., Hu, A., and Nadiga, B. T.: CMIP6 Models Predict Significant 21st Century Decline of the Atlantic Meridional Overturning Circulation, Geophysical Research Letters, 47, e2019GL086 075,

530   https://doi.org/https://doi.org/10.1029/2019GL086075, 2020.

Wett, S., Rhein, M., Kieke, D., Mertens, C., and Moritz, M.: Meridional Connectivity of a 25-Year Observational AMOC Record at 47°N, Geophysical Research Letters, 50, e2023GL103 284, https://doi.org/https://doi.org/10.1029/2023GL103284, 2023.

Wood, R. A., Rodríguez, J. M., Smith, R. S., Jackson, L. C., and Hawkins, E.: Observable, low-order dynamical controls on thresholds of the Atlantic meridional overturning circulation, Climate Dynamics, 53, 6815–6834, https://doi.org/10.1007/s00382-019-04956-1, 2019.

535   Yang, Q., Dixon, T. H., Myers, P. G., Bonin, J., Chambers, D., van den Broeke, M. R., Ribergaard, M. H., and Mortensen, J.: Recent increases in Arctic freshwater flux affects Labrador Sea convection and Atlantic overturning circulation, Nature Communications, 7, 10 525, https://doi.org/10.1038/ncomms10525, 2016.

Zhang, R. and Thomas, M.: Horizontal circulation across density surfaces contributes substantially to the long-term mean northern Atlantic Meridional Overturning Circulation, Communications Earth & Environment, 2, 112, https://doi.org/https://doi.org/10.1038/s43247-021-00182-y, 2021.

540   Zhu, C. and Liu, Z.: Weakening Atlantic Overturning Circulation Causes South Atlantic Salinity Pile-up, Nature Climate Change, 10, 998–1003, https://doi.org/10.1038/s41558-020-0897-7, 2020.

Zhu, C., Liu, Z., Zhang, S., et al.: Likely accelerated weakening of Atlantic overturning circulation emerges in optimal salinity fingerprint, Nature Communications, 14, 1245, https://doi.org/10.1038/s41467-023-36288-4, 2023.

545   Årthun, M., Brakstad, A., Dörr, J., Johnson, H. L., Mans, C., Semper, S., and Våge, K.: Atlantification drives recent strengthening of the Arctic overturning circulation, Science Advances, 11, eadu1794, https://doi.org/10.1126/sciadv.adu1794, 2025.